

Atomic hydrogen adsorption and incipient hydrogenation of the Mg(0001) surface: A density-functional theory study

Yanfang Li,¹ Ping Zhang,^{2,*} Bo Sun,² Yu Yang,² and Yinghui Wei¹

¹*College of Materials Science and Engineering,*

Taiyuan University of Technology, Taiyuan 030024, People's Republic of China

²*LCP, Institute of Applied Physics and Computational Mathematics,*

P.O. Box 8009, Beijing 100088, People's Republic of China

Abstract

We investigate the atomic hydrogen adsorption on Mg(0001) by using density-functional theory within the generalized gradient approximation and a supercell approach. The coverage dependence of the adsorption structures and energetics is systematically studied for a wide range of coverage Θ (from 0.11 to 2.0 monolayers) and adsorption sites. In the coverage range $0 < \Theta < 1.0$, the most stable among all possible adsorption sites is the on-surface fcc site followed by the hcp site, and the binding energy increases with the coverage, thus indicating the higher stability of on-surface adsorption and a tendency to the formation of H islands (clusters) when increasing the coverage within the region $0 < \Theta < 1.0$. The on-surface diffusion path energetics of atomic hydrogen, as well as the activation barriers for hydrogen penetration from the on-surface to the subsurface sites, are also presented at low coverage. At high coverage of $1.0 < \Theta \leq 2.0$, it is found that the coadsorption configuration with 1.0 monolayer of H's residing on the surface fcc sites and the remaining $(\Theta - 1.0)$ monolayer of H's occupying the subsurface tetra-I sites is most energetically favourable. The resultant H-Mg-H sandwich structure for this most stable coadsorption configuration displays similar spectral features to the bulk hydride MgH₂ in the density of states. The other properties of the H/Mg(0001) system, including the charge distribution, the lattice relaxation, the work function, and the electronic density of states, are also studied and discussed in detail. It is pointed out that the H-Mg chemical bonding during surface hydrogenation displays a mixed ionic/covalent character.

PACS numbers: 68.43.Bc, 68.43.Fg, 68.43.Jk, 73.20.Hb

*Corresponding author; zhang_ping@iapcm.ac.cn

I. INTRODUCTION

The interaction between the hydrogen and the magnesium has long received many experimental [1, 2, 3, 4, 5, 6, 7, 8, 9, 10, 11, 12, 13, 14] and theoretical [14, 15, 16, 17, 18, 19, 20, 21, 22, 23, 24, 25, 26] concerns, especially due to the fact that hydrogen is the best candidate of clean fuel in the future and Mg is an important potential hydrogen storage material. One key blockade to prevent Mg from practical application in hydrogen storage is its high reaction temperature and kinetic barrier for hydrogenation and dehydrogenation [27]. However, recent systematic experiments [1, 2, 3, 14, 19] have shown that the hydrogen reaction kinetics can be prominently improved by adding transition elements (such as Ni, Ti) as catalyst in the magnesium hydride (MgH_2). Along this line many interesting phenomena have been found, for example, it has been shown that alloying Mg with Ni can weaken the bonding between H and Mg atoms and thus favor H_2 adsorption/dissociation process.

On the other hand, a thorough understanding of the atomic H adsorption on the Mg surface from basic quantum-mechanical viewpoint is still lacking, although some scarce theoretical [14, 15, 16, 17, 18] and experimental [10, 11, 12, 13, 14] data have been existed in previous reports. In particular, the coverage dependence of the Mg-H bonding properties is highly interesting but remains yet to be fully studied. Motivated by this observation, in this paper, we present a first-principles study by systematically calculating the coverage dependence of atomic hydrogen structures on the Mg(0001) surface and subsurface in a variety of coverage range from 0.11 to 2.0 monolayer (ML). Through these energetics calculations, we analyze and discuss the atomic hydrogen adsorption structures, the Mg-H chemical bonding properties, and the surface diffusion and penetration energetics of atomic hydrogen on Mg(0001). By comparing the binding energies and the adsorption behavior at different coverages, we obtain the saturation coverage of 1.0 ML on surface and find the spontaneously relaxed H-Mg-H sandwich structure at the coverage larger than 1.0 ML. On the whole, our present systematic first-principles study provides a detailed enlightening information of the incipient hydrogenation of Mg(0001).

The rest of this paper is organized as follows: In Sec. II, we describe our first-principle calculation method and the models used in this paper. In Sec. III, we present in detail our calculated results, including the on-surface and subsurface H adsorption energies in a wide range of coverage, the structures and properties of the H-Mg bonds, and the surface

diffusion and penetration energetics. At last, the conclusion is given in Sec. IV.

II. COMPUTATIONAL METHOD

The first-principles calculations based on the density functional theory (DFT) are performed using the Vienna *ab initio* simulation package [28] (VASP) with the projector-augmented-wave (PAW) pseudopotentials [29] and plane waves. The plane-wave energy cutoff was set to 250 eV. The so-called *repeated slab* geometries are applied. This scheme consists of the construction of a unit cell of an arbitrarily fixed number of atomic layers identical to that of the bulk in the plane of the surface (defining the bidimensional cell), but symmetrically terminated by an arbitrarily fixed number of empty layers (the “*vacuum*”) along the direction perpendicular to the surface. In the present study, the clean Mg(0001) surface is modeled by periodic slabs consisting of nine magnesium layers separated by a vacuum of 20 Å, which is found to be sufficiently convergent [20]. The hydrogen atoms are adsorbed on both sides of the slab in a symmetric way. During our calculations, the outermost three magnesium layers, as well as the H atoms, are allowed to relax while the central three layers of the slab are fixed in their calculated bulk positions. If not mentioned differently we have used a $(15 \times 15 \times 1)$ k -point grid for the $p(1 \times 1)$ surface cell, $(9 \times 9 \times 1)$ k -point grid for the $p(\sqrt{3} \times \sqrt{3})$ and $p(2 \times 2)$ cells, and $(7 \times 7 \times 1)$ k -point grid for the $p(3 \times 3)$ cell, with Monkhorse-Pack scheme [30]. Furthermore, the generalized gradient approximation (GGA) of Perdew *et al.* [31] for the exchange-correlation potential is employed. A Fermi broadening [32] of 0.02 eV is chosen to smear the occupation of the bands around E_F by a finite- T Fermi function and extrapolating to $T=0$ K.

In the present paper, the calculations for hydrogen atoms in the seven adsorption sites, including on-surface (top, hcp, fcc, and bridge) and subsurface (tetra-I, tetra-II, and octa) sites depicted in Fig. 1, have been performed for coverage ranging from 0.11 to 2.0 ML. Specially, the hydrogen coverage of 0.11 ML and 0.33 ML are calculated using $p(3 \times 3)$ surface unit cell, while the coverage of 0.25, 0.5, 0.75, 1.0, 1.25, 1.5, 1.75 and 2.0 ML are calculated in the $p(2 \times 2)$ surface cell. The on-surface top and bridge adsorption sites are found to be unstable by the fact that the hydrogen atom initially located on these two sites will always move to the fcc site after relaxation. The subsurface tetra-I site at low coverage is also found to be unstable against the relaxation. Actually, the H atom placed on this

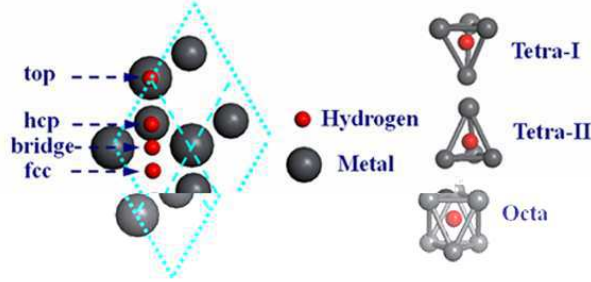


FIG. 1: (Colour online). (Left panel) Four on-surface adsorption sites including fcc, hcp, bridge and on-top sites. (Right panel) Three subsurface adsorption sites including tetra-I, tetra-II and octa sites. Note that Mg atoms of out layers are shown by scaled grey balls.

subsurface site will penetrate upward to a surface site after relaxation. Thus in this paper, most of the on-surface adsorption studies are focused on the fcc and hcp sites, while for the subsurface adsorption, the tetra-II and octa sites are mainly considered.

One central quantity tailored for the present study is the average binding energy of the adsorbed hydrogen atom defined as

$$E_b(\Theta) = -\frac{1}{N_H} [E_{\text{H/Mg}(0001)} - E_{\text{Mg}(0001)} - N_H E_H], \quad (1)$$

where N_H is the total number of H adatom present in the supercell at the considered coverage Θ (we define Θ as the ratio of the number of adsorbed atoms to the number of atoms in an ideal substrate layer). $E_{\text{H/Mg}(0001)}$, $E_{\text{Mg}(0001)}$, and E_H are the total energies of the slabs containing hydrogen, of the corresponding clean Mg(0001) slab, and of a free (spin polarized) hydrogen atom, respectively. Thus a positive value of E_b indicates that the adsorption is exothermic (stable) with respect to a free H atom and a negative value indicates endothermic (unstable) reaction. On the other hand, since in most cases, the hydrogen chemisorption process inevitably involves the dissociation of H_2 molecules, thus the adsorption energy per hydrogen atom can alternatively be referenced to the energy which the H atom has in the H_2 molecule by subtracting half the dissociation energy D of the H_2 molecule,

$$E_{\text{ad}(1/2\text{H}_2)} = E_b - D/2. \quad (2)$$

With this choice of adsorption energy, then a positive value indicates that the dissociative adsorption of H_2 is an exothermic process, while a negative value indicates that it is endothermic and that it is energetically more favorable for hydrogen to be in the gas phase as H_2 .

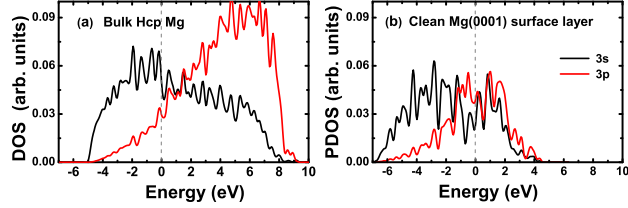


FIG. 2: (Color online). (a) The orbital-resolved DOS of bulk Mg and (b) the orbital-resolved site-projected DOS for top layer of the clean $p(1\times 1)$ -Mg(0001) film. The Fermi energy is set at zero.

III. RESULTS AND DISCUSSION

A. Bulk Mg and clean Mg(0001) surface

Before studying the H adsorption on the Mg(0001) surface, we first consider the bulk Mg and clean Mg(0001) surface. Our calculated lattice parameters for bulk hcp Mg are $a=3.207$ Å and $c/a=1.60$, well comparable to the experimental values of 3.21 Å and 1.62 [33, 34]. The calculated cohesive energy is -1.52 eV/atom, also in good agreement with the experimental value of -1.51 eV/atom [33, 34]. The orbital-resolved electronic density of states (DOS) per atom for the bulk Mg is shown in Fig. 2(a) with the Fermi energy set at zero. The two broad peaks correspond to Mg 3s and 3p states, which are heavily mixed each other near the Fermi energy. This s - p orbital mixing results from the characteristic hcp structure of bulk Mg in its ground state. In addition, the distribution form of the total DOS in a wide energy range of -5.0 eV $< E < 4.0$ eV can be nearly considered as a function of $E^{1/2}$, which is also a typical feature of the sp -hybrid simple metals.

The calculation for the atomic relaxations of the clean surface with 1×1 , $\sqrt{3}\times\sqrt{3}$, 2×2 , and 3×3 periodicities provides not only a test of the clean surface with different cell sizes, but is also used to evaluate the charge density difference used later and assess the changes in the work function by hydrogen adsorption. Our clean-surface calculation shows that the two outermost Mg(0001) layers relax significantly from the bulk values. The first-second interlayer expansion is nearly 2% and the second-third interlayer expansion is about 0.58%, which compares well with recent first-principles results [18, 23]. Note that the first interlayer separation on most metal surfaces is contracted. From this aspect, Mg(0001) is an anomalous example showing the outermost interlayer expansion, which has been proved and interpreted

TABLE I: The calculated results of the surface energy E_s (eV) and the work function Φ (eV) for the clean Mg(0001) surfaces in different k -point meshes.

model	k -point mesh	E_s (eV)	Φ (eV)
1×1	$12 \times 12 \times 1$	0.2911	3.711
1×1	$15 \times 15 \times 1$	0.2947	3.729
2×2	$7 \times 7 \times 1$	0.2892	3.717
2×2	$9 \times 9 \times 1$	0.2977	3.733
$\sqrt{3} \times \sqrt{3}$	$7 \times 7 \times 1$	0.2881	3.701
$\sqrt{3} \times \sqrt{3}$	$9 \times 9 \times 1$	0.2951	3.728
3×3	$7 \times 7 \times 1$	0.2936	3.723
3×3	$9 \times 9 \times 1$	0.2911	3.704

by Staikov *et al.* [21]. The calculated charge density $n(\mathbf{r})$ (not depicted here) of the clean Mg(0001) surface shows that similar to the other typical metal surfaces [35], there is a rapid variation in $n(\mathbf{r})$ in the surface interstitial region, with $n(\mathbf{r})$ falling off sharply in magnitude toward the vacuum and soon “healing” the discrete atomic nature. This sizable charge redistribution near the surface is associated with the formation of the (uniform) surface dipole layer, which sensitively determines the work function. As one knows, the surface calculation requires enough k -point meshes, efficient energy cutoff, the correct model, and the other details to be the minimum numerical errors. To test the convergency of the physical properties of the clean Mg(0001) surface, we have calculated the surface energy E_s and the work function Φ of the clean Mg(0001) slabs by using different models with various k -point meshes. The results are listed in Table I, from which it reveals that the influences to the surface energetics from using different models are negligibly small. To keep the computation accuracy as high as possible for reliable comparison between different adsorption configurations, here we take to calculate and analyze surface energetics and electronic structures under the same model. For example, a $p(3 \times 3)$ surface unit cell is needed if one wants to analyze the properties of surface chemical activity in a coverage range beginning from $\Theta=0.11$.

Figure 2(b) plots the orbital-resolved site-projected density of states (PDOS) for the topmost Mg layer of the clean $p(1 \times 1)$ Mg(0001) surface cell. Compared to Fig. 2(a), one

can see that the surface electronic structure of the clean Mg(0001) differs from its bulk counterpart by a downward shift in PDOS and a decreasing charge occupation of the Mg $3p$ states. Note that throughout this paper, we do not consider the quantum size effects on the atomic and electronic structures, since in our various supercell models the substrate has been fixed with the same thickness.

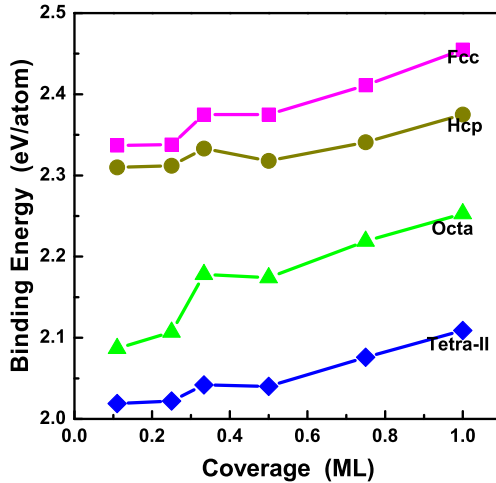


FIG. 3: (Color online). Calculated binding energy E_b of H/Mg(0001) system versus the coverage for the H atom adsorption in different sites. The solid lines connecting the calculated binding energies are used to guide the eyes.

B. Atomic hydrogen adsorption at $\Theta \leq 1.0$

First, we focus our attention to the hydrogen adsorption in the coverage regime $0 < \Theta \leq 1.0$. Keeping in mind the above-mentioned fact that the on-surface top and bridge, as well as the subsurface tetra-I site, is unstable for H adsorption in this coverage regime, our systematic calculations have been carried out for the remaining four high-symmetry adsorption sites, i.e., the on-surface fcc and hcp sites, together with the subsurface tetra-II and octa sites. The calculated binding energies E_b of H on these four on-surface and subsurface sites, with respect to the free atomic hydrogen, are illustrated in Fig. 3 and summarized in Table II for different hydrogen coverage in the regime $0 < \Theta \leq 1.0$. One can see that the binding energy for the on-surface adsorption is always larger than for the subsurface adsorption. Thus, in the coverage regime $0 < \Theta \leq 1.0$ the hydrogen on-surface adsorption is more energetically favourable than the subsurface adsorption, which indicates that the ad-H's will not spontaneously penetrate

TABLE II: The calculated binding energy E_b (in eV) and work function Φ (in eV) as functions of atomic hydrogen coverage on different sites of Mg(0001) surface.

	site	$\Theta=0.11$	0.25	0.33	0.50	0.75	1.0
E_b	Fcc	2.337	2.338	2.375	2.375	2.411	2.455
	Hcp	2.320	2.324	2.324	2.326	2.332	2.375
	Octa	2.020	2.022	2.035	2.050	2.086	2.109
	Tetra-II	2.047	2.217	2.218	2.224	2.230	2.209
Φ	Fcc	3.664	3.584	3.570	3.546	3.541	3.536
	Hcp	3.646	3.543	3.548	3.450	3.430	3.394
	Octa	3.698	3.645	3.669	3.593	3.569	3.539
	Tetra-II	3.691	3.610	3.627	3.498	3.357	3.302

into the subsurface in the case of pure on-surface adsorption. For the on-surface adsorption the fcc site is more stable than the hcp site, while for the subsurface adsorption the octa site is more favourable than the tetra-II site. Also, one can see from Fig. 3 that the binding energy increases with hydrogen coverage for all the four adsorption sites, which indicates a prominent attraction among the on-surface (or subsurface) ad-H's and implies a tendency to form H islands or clusters on the Mg(0001) surface (or subsurface) at $0 < \Theta < 1.0$. On the other hand, considering the binding energy E_b of hydrogen adatom with respect to the half of the binding energy for the H_2 molecule (the experimental value of 2.38 eV), the present calculations predict that in the whole coverage range we considered in this subsection, the atomic hydrogen on-surface (as well as subsurface) adsorption is stable. In addition, interestingly, the binding energy difference between the on-surface fcc and hcp sites, as well as between the subsurface octa and tetra-II sites, displays a noticeable increases with hydrogen coverage, which implies a substrate-induced anisotropy in the hydrogen-metal chemical bonding. Note that the changes of the binding energy E_b from 0.11 to 0.25 ML is not well linear with the coverage and the markable deviation occurs at 0.33 ML. This is a result of the effective interaction between the surface adsorbates.

To further clarify our observation that the hydrogen adsorbates tend to form clusters on the Mg(0001) surface at $0 < \Theta < 1.0$, here as one typical example, we consider two kinds of arrangements for H_{fcc} adsorbates at the same coverage $\Theta=0.33$. These two adsorbate

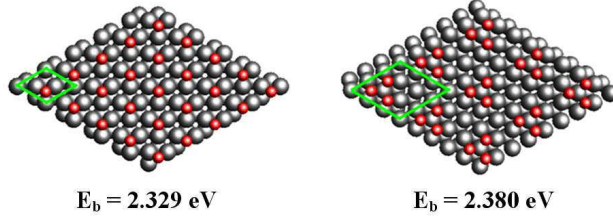


FIG. 4: (Color online). Two kinds of configurations for H_{fcc} adsorbates at the same coverage $\Theta=0.33$. The hydrogen adatoms in the right panel are arranged to be clustered, while in the left gives an uniform distribution. The calculated binding energies show that the adsorption in the right panel is more stable.

TABLE III: The calculated adsorbate height $h_{\text{H-Mg}}$, the bond length (R_a) and the interlayer relaxation (Δ_{12}) for different coverage of atomic hydrogen adsorption on Mg(0001) surface.

Coverage Θ	$h_{\text{H-Mg}}$		R_a (Å)		Δ_{12} (%)	
	Fcc	Hcp	Fcc	Hcp	Fcc	Hcp
0.11	0.917	0.901	2.012	2.034	2.025	2.730
0.25	0.822	0.803	2.014	2.015	1.916	2.108
0.33	0.817	0.818	1.984	1.987	1.890	1.978
0.5	0.888	0.871	2.010	2.013	1.764	2.104
0.75	0.856	0.854	2.031	2.035	1.108	1.818
1.0	0.837	0.835	2.032	2.045	-0.450	0.323

arrangements are shown in Fig. 4. The left panel in Fig. 4 corresponds to case of a $p(\sqrt{3}\times\sqrt{3})$ surface cell, while the right panel gives one selective adsorbate configuration produced from the $p(3\times 3)$ surface cell. Obviously, the hydrogen adatoms in the right panel are more clustered than those in the left panel. Remarkably, the calculated binding energy is $E_b=2.329$ eV for the left panel and $E_b=2.380$ eV for the right panel, which clearly shows the preference for the formation of hydrogen clusters on the Mg(0001) surface. Note that 1×1 H islands are unfavourable because of the electrostatic H-H repulsion, which will be discussed in Sec. III C.

Table III presents the calculated results for the relaxed atomic structure, including the height $h_{\text{H-Mg}}$ of H above the surface, the H-Mg bond length R_a , and the topmost interlayer relaxations Δ_{12} for various coverage with H in the fcc and hcp sites. One can see that the

adsorption of hydrogen on Mg(0001) induces notable changes in the interlayer distance of the substrate. In fact, the value of Δ_{12} monotonically decreases with hydrogen coverage for both fcc and hcp adsorption. For the fcc adsorption, in particular, the value of Δ_{12} even becomes negative at $\Theta=1.0$, which means that the topmost interlayer relaxation changes from expansion [about 2.0% for clean Mg(0001) surface] to contraction. This reflects the strong influence of the H adsorbates on the neighboring Mg atoms, and thus results from important redistribution of the electronic structure. Thus, our results verify that the hydrogen adsorption causes the Mg(0001) outmost layer separation to relax back to something close to its “ideal” bulk value. Concerning the H-Mg bond length R_a at different hydrogen coverage, one can see from Table III that for both fcc and hcp adsorption, the H-Mg bond length varies around 2.0 Å very little with increasing Θ . In particular, the calculated results of R_a by using the same $p(2\times 2)$ surface model vary only within an amplitude of 0.02 Å (0.03 Å) for fcc (hcp) site. The short bond length R_a implies a strong interaction between H and Mg atoms. Note that the value of R_a for H_{fcc} is slightly shorter than that for H_{hcp} , which is consistent with the fact that the fcc site is more stable than the hcp site for on-surface adsorption.

We turn now to analyze the electronic properties of the H/Mg(0001) system by first considering the work function Φ , which is plotted in Fig. 5 and summarized in Table II for different hydrogen coverage. For the clean Mg(0001) our calculated Φ has a typical value of 3.728 eV, which is well comparable to the previous calculations. From Fig. 5, it can be seen that the work function steadily decreases (within a relatively small variation range) with H coverage for both on-surface and subsurface adsorption. On the whole, the variation amplitude of the work function is relatively small, which can be associated with the small adsorption distance for the H species. The decreasing linetype and amplitude of Φ shown in Fig. 5 as a function of Θ depend on the adsorption configuration. For the on-surface adsorption, one can see that the work function for the hcp adsorption is always lower than that for the fcc adsorption, and their difference increases with Θ , which means that the surface charge polarization effect is more prominent for the hcp adsorption than for the fcc adsorption in the whole coverage considered. For the subsurface adsorption, In a similar manner, the octa-adsorbed work function is always lower than that for the tetra-II adsorption, and their difference also increases with Θ . Interestingly, with increasing the hydrogen coverage, the value of work function for the on-surface fcc adsorption approaches

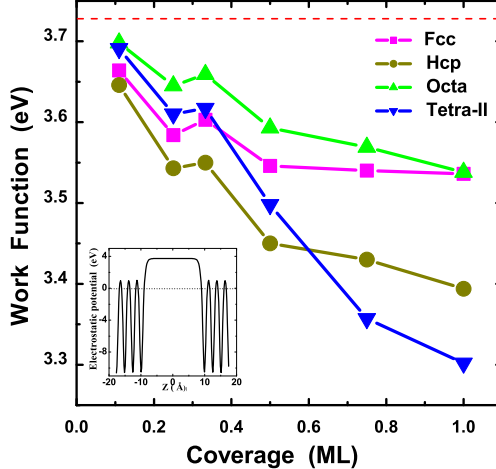


FIG. 5: (Color online). The calculated work function Φ versus the coverage for the H atom adsorption in different sites. The dashed line shows the value of Φ for clean Mg(0001) substrate. As an example, the inset shows the planar-averaged electrostatic potential of clean Mg(0001) slab, with the Fermi energy set at zero.

to have the same value as that for the subsurface octa adsorption.

To gain more insight into the nature of Mg-H bonding during the hydrogen adsorption onto Mg(0001) surface, we now analyze our results by means of the electron density difference $\Delta n(\mathbf{r})$, which is obtained by subtracting the electron densities of noninteracting component systems, $n_{\text{Mg}(0001)}(\mathbf{r}) + n_{\text{H}}(\mathbf{r})$, from the density $n(\mathbf{r})$ of the H/Mg(0001) system, while retaining the atomic positions of the component systems at the same location as in H/Mg(0001). Figure 6(a) and 6(b) present the contour plots of $\Delta n(\mathbf{r})$ for $\Theta=0.25$ and 1.0, respectively. One can see that the charge redistribution mainly occurs at the surface and involves in the H adatom and the topmost Mg atoms. It is apparent that upon adsorption, electrons flow from Mg *sp* metallic state into H 1s state, resulting in a depletion of the surface metallic electrons. With the increase in hydrogen coverage, it shows that (i) more Mg *sp* electrons transfer to the localized H 1s orbital, implying that ionicity of the Mg-H bonding increases with hydrogen coverage, and (ii) not only the topmost but also the second Mg atomic layer is prominently influenced by increasing the hydrogen coverage, which can be clearly seen by the charge redistribution shown in Fig. 6(b). On the other hand, there is also a weak but important covalent component in Mg-H chemical bonding (see Fig. 7 below for details). The unique signature of this covalency occurred in Fig. 6 is the orientation of

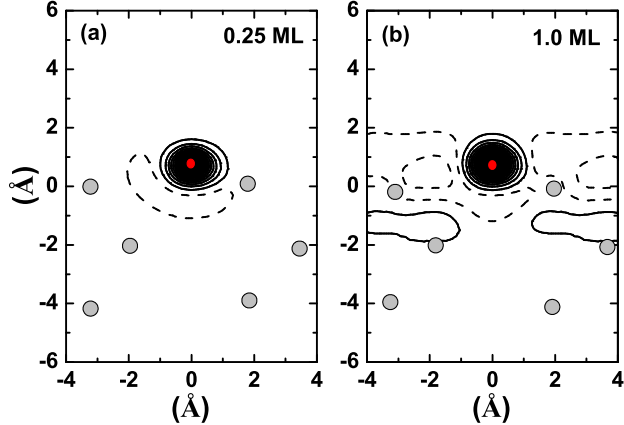


FIG. 6: (Color online). Contour plot of the charge density difference $\Delta n(\mathbf{r})$ for the on-surface H/Mg(0001) slab with hydrogen coverage (a) $\Theta=0.25$ and (b) $\Theta=1.0$. The solid (dashed) lines stand for the electron accumulation (depletion) regions. The red (gray) points stand for H and Mg atoms. The contour spacing is $0.02 \text{ electrons}/\text{\AA}^3$.

the charge accumulation (around H adatom), which, due to the hybridization of surface Mg sp and H $1s$ states, tends to point along the Mg-H bond. Thus, one can see that the chemical bonding between the surface Mg atom and H adatom is a mixture of ionic and covalent bonding. For pure MgH_2 with rutile structure, recent experimental and theoretical studies have shown that the bulk Mg-H chemical bonding also has a mixed ionic/covalent nature. Another fact shown in Fig. 6 is that like the other hydrogen/metal systems, the influence of the adsorbed Mg(0001) surface is rapidly screened out on going into the bulk. The bonding character of the inner Mg layers (from the second layer for $\Theta=0.25$ and from the third layer for $\Theta=1.0$) is essentially identical to the bulk case, which is typically metallic with a fairly constant charge density between the atoms with slight directional bonding along the body diagonals. This can be clearly seen in Fig. 6 which shows negligibly small changes in the interior of the nine-layer Mg slab at both low ($\Theta=0.25$) and high ($\Theta=1.0$) coverage.

Figures 7(a) and 7(b) show the orbital-resolved PDOS for the on-surface H_{fcc} layer and the topmost Mg layer at $\Theta=0.25$ and $\Theta=1.0$, respectively. The Fermi energy has been set at zero. At low coverage ($\Theta=0.25$), the narrow peak around -6.0 eV with large amplitude denotes H $1s$ state, which, as shown in Fig. 7(a), mainly hybridizes with the $3s$ state of the outmost Mg atoms. Whereas, the hybridization between H $1s$ and Mg $3p$ states is negligibly small. By comparing the low-coverage adsorbed [Fig. 7(a)] and clean [Fig. 2(b)] Mg(0001)

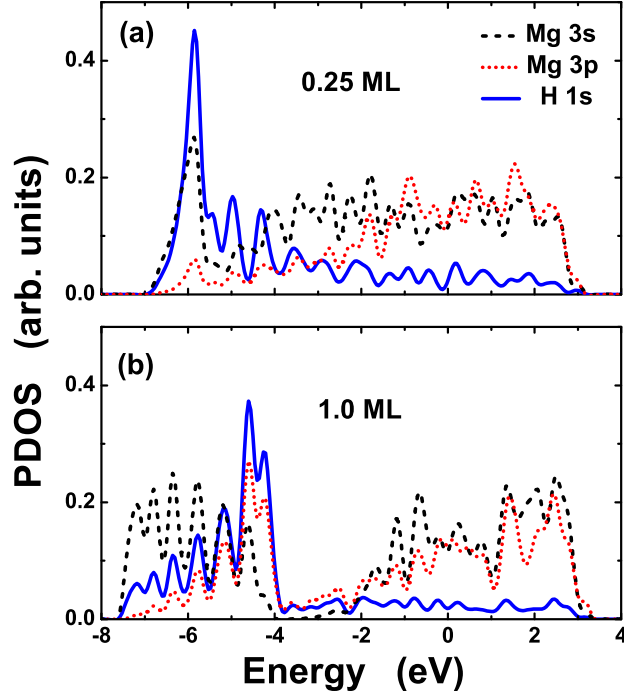


FIG. 7: (Color online). The PDOS for the on-surface H_{fcc} atoms and the topmost Mg layer at (a) $\Theta=0.25$ and (b) $\Theta=1.0$. The Fermi level is set at zero.

surfaces, one can see that the main change for the surface Mg layer upon the low-coverage hydrogen adsorption is the distinct enhancement of its 3s PDOS at the Mg valence band edge (around -6.0 eV) due to the bonding with H 1s state. At this moment, it is interesting to question why the electronic bonding of the hydrogen adatom and the surface Mg atoms occurs at the Mg valence band edge in the case of low adsorption coverage. The reason is simply because this band edge, as shown in Fig. 2(b), is dominated by the Mg 3s state, while the other part of the Mg valence band is a mixture of Mg 3s and 3p states. At low coverage, the H adatom has the low coordinates, which makes it favourable for the H(1s)-Mg(3s) chemical bonding. Thus, at low coverage the H adatom chooses to bond at the Mg valence band edge as shown in Fig. 7(a). With increasing hydrogen coverage [Fig. 7(b) for $\Theta=1.0$], three prominent changes involving the H-Mg chemical bonding occur: (i) the peak in the H 1s PDOS is broadened and shifts upward to go into the interior of the Mg valence band. These changes for the H 1s PDOS is due to the fact that at as high coverage as $\Theta=1.0$, the H adatom is highly coordinated, which drives the H 1s state to bond with not only the 3s state but also the 3p states of the topmost Mg atoms. Since the Mg 3p states

lies mainly in the interior of the valence band, thus the H 1s state has to shift up in energy to overlap with the Mg 3p states; (ii) Compared to case of $\Theta=0.25$, the hybridization of H 1s and Mg 3p states is distinctly enhanced in the case of $\Theta=1.0$. In particular, the main peak around $E=-4.5$ eV in the H 1s PDOS in Fig. 7(b) is a result of the hybridization between H 1s and Mg 3p states. The reason for this increasing H(1s)-Mg(3p) hybridization at high coverage has been clarified in (i); (iii) The distribution of Mg 3s and 3p states in the energy region $-4.0 < E < -2.0$ eV tends to vanish due to a large weight transfer of these states to more lower energy, which is caused by the formation of the bonding and antibonding states between H 1s and Mg *sp* atomic orbitals. This is most prominent for Mg 3s state. In fact, one can see from Fig. 7(b) that in the energy interval $-7.0 < E < -6.0$ eV there is a large filling of the surface Mg 3s state, which is empty in this energy region in the cases of clean [Fig. 2(b)] and low-coverage [Fig. 7(a)] Mg(0001) surfaces. Obviously, this state-transfer toward more lower energy in increasing adsorption coverage will gain the energy, which overcompensates the energy that is costed by the elevation of the H 1s state when increasing adsorption coverage. The net result is that the adsorption of the on-surface H_{fcc} at $\Theta=1.0$ is more stable than at $\Theta=0.25$, as has been shown in Fig. 3.

After clarifying the chemical bonding properties for the most stable hydrogen adsorption configuration, i.e., the on-surface fcc site, we turn now to study the diffusion energetics of the H adatom when it undergoes the in-plane diffusion and the inter-plane penetration (from surface to subsurface). Diffusion of atomic hydrogen after on-surface dissociation of H_2 is an elementary process during the surface hydrogenation process. Also, the hydrogen diffusion plays an important role in understanding many catalytic reaction. Here, by using the DFT total energy calculation, we report our numerical results of the energy barriers for atomic H diffusion and penetration in the H/Mg(0001) system.

Using the nudged elastic band (NEB) method, which will find the saddle points and minimum energy paths on complicated potential surface, we have calculated the surface diffusion-path energetics of atomic hydrogen. The results at $\Theta=0.25$ and $\Theta=1.0$ are shown in Fig. 8(a). Note that during calculation the number of atoms keeps invariant. Thus it also reveals in Fig. 8(a) the relative stability of H adsorption among various on-surface sites and the corresponding hydrogen binding energy differences. Our calculated diffusion barrier from fcc to hcp site is 0.33 eV at $\Theta=0.25$ and 0.18 eV at $\Theta=1.0$. The hcp site is less stable than the fcc site within the coverage $0 < \Theta \leq 1.0$. Thus the on-surface diffusion barrier from

hcp to fcc site presents an activation barrier with the value of 0.30 eV at $\Theta=0.25$ and 0.08 eV at $\Theta=1.0$. Therefore, we find that both the diffusion barrier from fcc to hcp site and activation diffusion barrier from hcp to fcc site is greatly decreased with coverage, which implies that at the coverage close to $\Theta=1.0$, the H/Mg(0001) surface at low temperature may display a mixed (disordered) phase that while the fcc sites are mainly occupied, there exist a small amount of ad-H's residing on the hcp sites due to thermal diffusion. On the other hand, the penetration-path energetics of surface ad-H's to the subsurface sites also sensitively depends on the coverage. Since the most favourable on-surface and subsurface adsorption sites are the fcc and octa sites respectively, also since there is no geometric obstacle between the neighboring fcc and octa sites, it is natural to speculate that at low temperature, the ad-H's on the surface fcc sites may penetrate to the neighboring subsurface octa sites through overcoming a relatively low barrier in the coverage range $0<\Theta\leq 1.0$. Thus, here we consider the energetics of this H penetration path. For this purpose, we fully relax the topmost three Mg layers step by step to search for the transition state with high energy. The calculated penetration path and the energy barrier from the on-surface fcc to subsurface octa site at two coverage ($\Theta=0.25$ and $\Theta=1.0$) is shown in Fig. 8(b), in which the horizontal coordinate indicates the penetration distance of the H atom with respect to the topmost Mg layer. At the low coverage of $\Theta=0.25$, the calculated barrier for fcc \rightarrow octa penetration is as large as 0.45 eV. The transition state, i.e., the atomic geometry of the energy maximum in the penetration path, correspond to the hydrogen atom in the surface Mg layer. When the coverage is increased to $\Theta=1.0$, as shown in Fig. 8(b), it is surprisingly found that the barrier is further increased to 0.75 eV. This is unlike the case of surface diffusion shown in Fig. 8(a), in which the energy barrier is weakened by increasing the adsorption coverage. Therefore, in contrast with one's intuitive expectation, our calculated results in Fig. 8(b) shows that the probability of low-temperature interlayer penetration is negligibly small in the coverage range $0<\Theta\leq 1.0$.

C. Atomic hydrogen adsorption at $1.0<\Theta\leq 2.0$

From above discussions, one can see that in the coverage range $0<\Theta\leq 1.0$, the most stable adsorption site for H/Mg(0001) system is the on-surface fcc site. To penetrate into the interior of the magnesium substrate, the hydrogen adatom has to overcome a large-

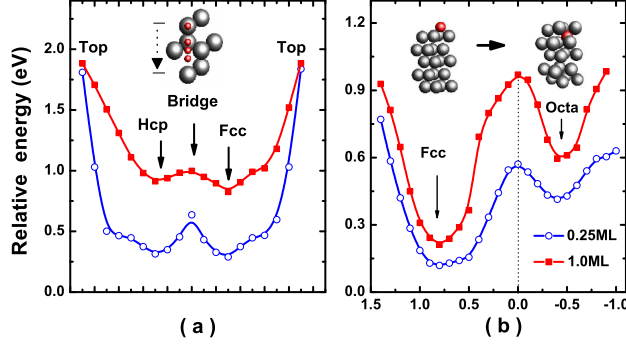


FIG. 8: (Color online). (a) The surface diffusion and (b) penetration (from on-surface fcc to subsurface octa site) energetics for the H adatom on the Mg(0001) with the coverage of 0.25 and 1.0 ML, respectively. The insets schematically plot atomic geometries along the diffusion and penetration pathes.

amplitude (~ 0.75 eV) energy barrier, which has been shown in Fig. 8(b) for the energy path from the on-surface fcc to the subsurface octa site. This means that at low temperature, the H adatoms will mostly reside on the Mg(0001) surface and a spontaneous penetration process cannot occur at $0 < \Theta \leq 1.0$. Then, one may naturally ask an important question: what will happen when the hydrogen coverage is more than 1.0 ML, or what is the saturation coverage for surface adsorption? This question is closely related to the clear understanding of the surface hydrogenation of magnesium and is answered in the following discussions by calculating the hydrogen adsorption energetics in the coverage range $1.0 < \Theta \leq 2.0$. One should notice that up to now the exact knowledge of saturation coverage is still unreasonable experimentally because of the limitation of the resolution and device factors. Theoretical study and prediction of surface hydrogenation are thus still particularly enlighting at the present stage.

To study the hydrogen adsorption in the coverage range $1.0 < \Theta \leq 2.0$ with allowable computation time, we choose a $p(2 \times 2)$ supercell to construct four coverage configurations, i.e., $\Theta = 1.25, 1.5, 1.75,$ and 2.0 . The initial positions of H atoms for relaxation calculation are set such that one ML of H atoms are placed on the surface fcc sites of Mg(0001), then the remaining $(\Theta - 1.0)$ ML of H's are placed on the surface hcp sites of Mg(0001), see Fig. 9(a) for the top and side view of one selective initial atomic geometry ($\Theta = 2.0$). This choice of initial geometries is simply motivated by the above low-coverage result that the on-surface

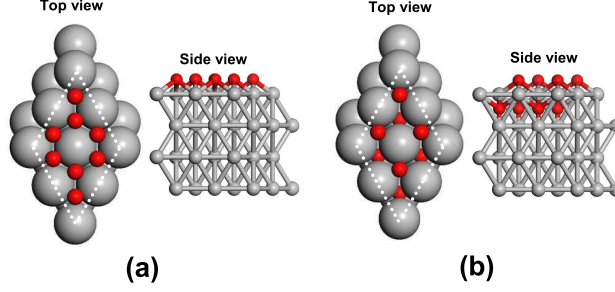


FIG. 9: (Color online). (a) The initial structure (4fcc+4Hcp) and (b) the end structure (4fcc+4Tetra-I) in the relaxation of H/(2×2)-Mg(0001) system with 2.0ML coverage.

TABLE IV: Calculated binding energies E_b (in eV) and the interlayer relaxation (Δ_{12} and Δ_{23}) for atomic hydrogen adsorption on Mg(0001) surface at coverage of $1.0 < \Theta \leq 2.0$.

Θ	1.25	1.5	1.75	2.0
$\Delta_{12}(\%)$	2.266	5.738	9.373	13.30
$\Delta_{23}(\%)$	0.179	1.452	2.628	3.50
E_b (eV)	2.504	2.518	2.515	2.511

fcc and hcp sites are more stable than the subsurface tetra-II and octa sites. Then, the total-energy relaxation calculation is carried out in the same manner as that in the above discussion. After atomic relaxation, prominently, we find that the H atoms initially placed on the surface hcp sites spontaneously move to the subsurface tetra-I site [see Fig. 9(b)] without encountering any penetration barrier. The driving force for this spontaneous penetration process may be due to the mutual repulsion of high-coverage H adatoms. This reasoning is consistent with the partially-ionic chemical bonding between H and Mg atoms, which results in a negative charge carried by H's and thus generates a repulsion among these adsorbates. Thus, we arrive at a conclusion that within the coverage range $1.0 < \Theta \leq 2.0$, the surface and subsurface of Mg(0001) are coadsorbed, with 1.0 ML of H's residing on the surface sites and $(\Theta - 1.0)$ ML of H's occupying the subsurface tetra-I sites.

Even more interestingly, we find that this coadsorption of both on-surface and subsurface sites is energetically more favourable than the pure on-surface or subsurface adsorption. This can be seen from Table IV, in which the calculated hydrogen binding energies for $\Theta = 1.25, 1.5, 1.75$ and 2.0 (with the above-mentioned initial geometries) are listed. By comparing with the binding energy data listed in Table II, one can see from Table IV that

the hydrogen high-coverage coadsorption at $1.0 < \Theta \leq 2.0$ [with 1.0 ML H's residing on the surface sites and $(\Theta - 1.0)$ ML H's occupying the subsurface tetra-I sites] is more stable than the pure on-surface or subsurface adsorption at $0 < \Theta \leq 1.0$. Note that there also exists many stable coadsorption configurations in the coverage range $0 < \Theta \leq 1.0$. We have systematically calculated the total energies of these low-coverage coadsorption configurations. For example, for $\Theta = 0.5$ we have used the $p(2 \times 2)$ supercell to construct the following three coadsorption geometries: (i) one H is on the surface fcc site and the other one H is on the subsurface tetra-I site; (ii) one H is on the surface fcc site and the other one H is on the subsurface tetra-II site; (iii) one H is on the surface fcc site and the other one H is on the subsurface octa site. For the other coverage satisfying $0 < \Theta \leq 1.0$, the coadsorption configurations are constructed in a similar manner. Our systematic calculations clearly show that within the coverage range $0 < \Theta \leq 1.0$, the coadsorption is less stable than the pure on-surface fcc adsorption. Combining the results for both $0 < \Theta \leq 1.0$ and $1.0 < \Theta \leq 2.0$, therefore, we get a critical coverage value of $\Theta = 1.0$ for hydrogen adsorption on Mg(0001). Below this value the ad-H's occupy the on-surface fcc sites, while above this value ($1.0 < \Theta \leq 2.0$), 1.0 ML of H's occupy the on-surface fcc sites and the remaining $(\Theta - 1.0)$ ML of H's occupy the subsurface tetra-I sites. Here, the occupation of the subsurface tetra-I sites can be understood as a result of the spontaneous penetration process of the on-surface H_{hcp} adatoms, provided the on-surface fcc sites are fully occupied. As has been mentioned above, the driving force for this spontaneous penetration process is possibly from the repulsion of the neighboring on-surface ad-H dipoles. Dipole-dipole repulsion is a mechanism that has been proposed to explain how surface oxidation begins. Remarkably, our present results clearly show a similar mechanism responsible to the incipient hydrogenation of Mg(0001) surface.

Now let us turn back to Table IV, in which, besides the H adsorption energy, also presents the first and second interlayer relaxations (Δ_{12} and Δ_{23}), as well as the H-Mg bond length R_a , for the relaxed atomic structures of four coverage in the region $1.0 < \Theta \leq 2.0$. Prominently, one can see that the coadsorption of hydrogen on Mg(0001) induces distinct changes in the interlayer distance of the substrate. In particular, the topmost interlayer relaxation changes from contraction $\Delta_{12} = -0.45\%$ at $\Theta = 1.0$ to expansion $\Delta_{12} = 13.3\%$ at $\Theta = 2.0$. This large change of atomic relaxations upon H coadsorption is largely ascribed to the occupation of ad-H's at the subsurface tetra-I sites, which together with the surface ad-H's, form a H-Mg-H sandwich structure and thus breaks metallic bonding between the first and second

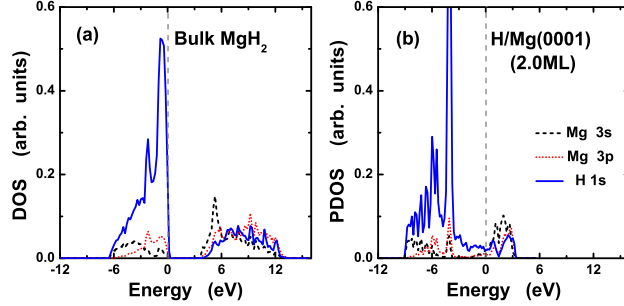


FIG. 10: (Color online). (a) The DOS of bulk MgH₂ and (b) the projected DOS for H-Mg-H sandwich structure of H/Mg(0001) at coverage $\Theta=2.0$. The energy is measured with reference to the Fermi level.

Mg(0001) atomic layers. Because of this large interlayer expansion one can speculate that this H-Mg-H sandwich structure is a precursor in the process of H-induced embrittlement and ablation of Mg(0001). Needless to say, larger interlayer expansion costs more energy, which will counteract the formation of H/Mg(0001) structures of more higher coverage. This statement is supported by the result shown in Table IV that the binding energy E_b arrives at its maximum at $\Theta=1.5$. Based on this observation, in this paper we do not consider the coverage region of $\Theta>2.0$.

To help understand the hydrogenation of Mg(0001), which is characterized by the occurrence of surface hydride, it is instructive to compare the electronic properties of the present H-Mg-H sandwich structures and the bulk hydride MgH₂. For this we have calculated the ground-state properties of the bulk MgH₂ with rutile structure. Our optimized lattice parameters and internal coordinate parameters are in good agreement with the experimental data [16]. Then, we calculate and plot in Fig. 10(a) the orbital-resolved PDOS of H and Mg in MgH₂. One can see that MgH₂ is an insulator with a band gap of 4.0 eV. The valence band is dominated by H 1s and the conduction band mainly consists of Mg *sp* states, which means that the Mg-H bonds in MgH₂ are mainly ionic. On the other hand, Fig. 10(a) also shows that a small amount of Mg *sp* states in the valence band hybridize with the H 1s state and contribute some covalent character to the bonding. It has been experimentally measured [16] that the ionic charge of Mg and H atoms in MgH₂ are represented Mg^{1.91+} and H^{0.26-}, which implies that the Mg and H atoms in MgH₂ are ionized in-equivalently. In other words, Mg is ionized almost as Mg²⁺, while H is very weakly ionized. Figure 10(b) plots the orbital-resolved PDOS for the present H-Mg-H sandwich structure of H/Mg(0001)

at coverage $\Theta=2.0$. In plotting Fig. 10(b) we have used the same number of H and Mg atoms as in Fig. 10(a). It can be seen that although there is an understandable difference in the spectral positions of H $1s$ and Mg sp states (relative to the Fermi energy) between the H-Mg-H sandwich structure of H/Mg(0001) and the bulk MgH_2 , the PDOS peak features for the two cases are yet very similar. For example, there are two prominent H $1s$ peaks below E_F for both the H-Mg-H sandwich structure of H/Mg(0001) and the bulk MgH_2 ; the energy distance between these two peaks is also very comparable for the two cases. The band charge distribution around these two H $1s$ peaks (not shown here) also reveals the similarity between the two cases. Therefore, we expect that it is possible to form on Mg(0001) the surface hydride with the similar chemical stoichiometry as the bulk MgH_2 . From this perspective we can see that Mg(0001) is a good case for studying the hydrogenation (and dehydrogenation) performance.

IV. CONCLUSION

In summary, we have systematically investigated the adsorption of atomic hydrogen on Mg(0001) surface and subsurface, as well as the energy barriers for atomic H diffusion and penetration in these systems through first-principles DFT-GGA calculations. We have considered a wide range of coverage from 0.11 to 2.0 ML by using different surface models [i.e., $p(3\times 3)$, $p(2\times 2)$, $p(\sqrt{3}\times\sqrt{3})$ and $p(1\times 1)$ surface unit cells] for adsorption in the on-surface fcc and hcp sites, as well as in the subsurface tetra-I, tetra-II, and octa sites. In the coverage range $0<\Theta\leq 1.0$, the most stable among all possible pure adsorbed sites, as well as coadsorbed sites, is the on-surface fcc site, followed by the hcp site. The atomic geometry, the work-function change, the charge density distribution, and the electronic structure upon the H adsorption have also been studied, which consistently show the fundamental influence by the ionic as well as covalent bonding between the H adatom and surface Mg atoms. Remarkably, this influence in the energetics is increased with increasing the H coverage, which is highly interesting. For instance, the increase in the H binding energy for the fcc or hcp site with Θ in the low coverage range ($0<\Theta<1.0$) implies the effective attraction between the H adsorbates, which will make it favourable for the formation of the hydrogen island or cluster *at low coverage less than one monolayer*. It should be stressed that the 1×1 H island is unfavourable because of the electrostatic H-H repulsion. Furthermore, in the low

coverage region $0 < \Theta \leq 1.0$ we have also calculated the surface diffusion as well as surface-to-subsurface penetration path energetics. For the on-surface diffusion, it has been found that the fcc and hcp sites are the two local minima, while the bridge is saddle point along the diffusion path. The activation barrier for the surface diffusion from hcp to fcc site is 0.30 eV at $\Theta=0.25$ and 0.08 eV at $\Theta=1.0$, implying that with increasing the hydrogen coverage in the region $0 < \Theta \leq 1.0$, the surface diffusion tends to be more easier. On the contrary, the activation barrier for the penetration from the on-surface fcc to the subsurface octa site is largely increased with increasing the hydrogen coverage. Thus, we have found that although the octa site is most stable for the pure subsurface adsorption, it is actually very hard to be reached at for H adatoms after dissociation of H_2 on Mg(0001) surface. This fact, together with the observation that the binding energy for the most stable on-surface fcc site does not saturate at $0 < \Theta \leq 1.0$, has motivated us to study hydrogen adsorption properties at more higher coverage of $1.0 < \Theta \leq 2.0$.

In the coverage range $1.0 < \Theta \leq 2.0$ and starting with the initial adsorption configurations that 1.0 ML of H's are placed on the surface fcc sites and $(\Theta - 1.0)$ ML of H's are placed on the surface hcp sites, we have found that after atomic relaxation, while the fcc H's keep the same sites, the hcp H's however undergo spontaneous penetration to the subsurface tetra-I sites, which are otherwise the unstable sites for the pure subsurface adsorption. This spontaneous penetration phenomenon is ascribed to the strong electrostatic H-H repulsion at $1.0 < \Theta \leq 2.0$. More interestingly, this final coadsorption configuration with 1.0 ML of H's residing on the surface fcc sites and the remaining $(\Theta - 1.0)$ ML of H's occupying the subsurface tetra-I sites is believed to be the most stable coadsorption configuration, after having compared its formation energy to those of a large number of other coadsorption configurations. In addition, the resultant H-Mg-H sandwich structure for this most stable coadsorption configuration has been shown to display similar DOS spectral features to the bulk hydride MgH_2 . Thus, we believe the present calculated results may greatly help understand the incipient hydrogenation of Mg(0001) surface.

Acknowledgments

P.Z. was supported by the NSFC under Grants No. 10604010 and No. 60776063. Y.W. was supported by the NSFC under Grants No. 50471070 and No. 50644041.

-
- [1] N. Hanada, T. Ichikawa and H. Fuji, *J. Phys. Chem. B* **109**, 7188 (2005); N. Hanada, T. Ichikawa, S. Orimo, and H. Fujii, *J. Alloys Compd.* **366**, 269 (2004).
- [2] G. Liang, J. Huot, S. Boily, A. Van Neste, and R. Schulz, *J. Alloys Compd.* **292**, 247 (1999); G. Liang, *J. Alloys Compd.* **370**, 123 (2004).
- [3] C. X. Shang, M. Bououdina, Y. Song, and Z. X. Guo, *Int. J. Hydrogen Energy* **29**, 73 (2004).
- [4] A. Zaluska, L. Zaluski, and J. O. Ström-Olsen, *J. Alloys Compd.* **288**, 217 (1999); A. Zaluska and L. Zaluski, *J. Alloys Compd.* **404**, 706 (2005).
- [5] W. Oelerich, T. Klassen, and R. Bormann, *J. Alloys Compd.* **322**, L5 (2001). W. Oelerich, T. Klassen and R. Bormann, *J. Alloys Compd.* **315**, 237 (2001);
- [6] J. F. Pelletier, J. Huot, M. Sutton, R. Schulz, A. R. Sandy, L. B. Lurio, and S. G. J. Mochrie, *Phys. Rev. B* **63**, 052103 (2001).
- [7] G. Barkhordarian, T. Klassen and R. Bormann, *Scr. Mater.* **49**, 213 (2003); G. Barkhordarian, T. Klassen and R. Bormann, *J. Alloys Compd.* **364**, 242 (2004).
- [8] D. Fatay, A. Revesz and T. Spassov, *J. Alloys Compd.* **399**, 237 (2005).
- [9] M Pozzo, D Alfè A Amieiro, S French, A Pratt, *J. Chem. Phys.* **128**, 094703 (2008).
- [10] J Renner and HJ Grabke, *Z. Metallk* **69**, 639 (1978).
- [11] J. Töpler, H. Buchner, H. Säufferer, K. Knorr, and W. Prandl, *J. Less-Common Met.* **88**, 397 (1982)
- [12] P. Spatz, A. Aebischer, A. Krozer, and L. Sclapbach, *Z. Phys. Chem.* **181**, 955 (1993).
- [13] PT Sprunger and EW Plummer, *Chem. Phys. Lett.* **187**, 559 (1991); PT Sprunger and EW Plummer, *Surf. Sci.*, **307**, 118 (1994).
- [14] T. Vegge, L. S. Hedegaard-Jensen, J. Bonde, T. R. Munter, and J. K. Nøskov, *J. Alloys Compd.* **386**, 1 (2005); T. Vegge, *Phys. Rev. B* **70**, 035412 (2004).
- [15] N. Jacobson, B. Tegner, E. Schröer, P. Hyldgaard, and B. I. Lundqvist, *Comput. Mater. Sci.*, **24**, 273 (2002).
- [16] T. Noritake, M. Aoki, S. Towata, Y. Seno, Y. Hirose, E. Nishibori, M. Takata, and M. Sakata, *Appl. Phys. Lett.* **81**, 2008 (2002);
- [17] N. Ohba, K. Miwa, T. Noritake, and A. Fukumoto, *Phys. Rev. B* **70**, 035102 (2004).
- [18] G. Wu, J. Zhang, Y. Wu., Q. Li., G. Zhou and X. Bao, *Acta Phys.-Chim. Sin.*, **24**(1), 55-60

- (2008).
- [19] Y. Song, Z. X. Guo, and R. Yang, Phys. Rev. B **69**, 094205 (2004).
 - [20] H. Song, P. Zhang, and X.-G. Zhao, Acta Phys. Sin., **56**, 465 (2007); X. Li, P. Zhang, and C. K. Chan, Physica B, **390**, 225 (2007).
 - [21] P Staikov, TS Rahman, Phys. Rev. B **60**, 15613 (1999).
 - [22] S. Li, P. Jena, and R. Ahuja, Phys. Rev. B **74**, 132106 (2006).
 - [23] E. Wachowicz, A. Kiejna J. Phys.: Condens. Matter., **13**, 10767 (2001).
 - [24] J. K. Nøskov, A. Hømoller, P. K. Johansson, and B. I. Lundqvist, Phys. Rev. Lett. **46**, 257 (1981).
 - [25] M. Johansson, C. W. Ostefeld, and I. Chorkendorff, Phys. Rev. B **74**, 193408 (2006).
 - [26] S. C. Bădescu, K. Jacobi, Y. Wang, K. Bedüftig, G. Ertl, P. Salo, T. Ala-Nissila and S. C. Ying, Phys. Rev. B **68**, 205401 (2003).
 - [27] JL Bobet, C. Even, Y. Nakamura, E. Akiba and B. Darriet, J. Alloys Compd. **298**, 279 (2000).
 - [28] G. Kresse and J. Furthmüller, Phys. Rev. B **54**, 11169 (1996).
 - [29] G. Kresse and D. Joubert, Phys. Rev. B **59**, 1758 (1999).
 - [30] H.J. Monkhorst and J.D. Pack, Phys. Rev. B **13**, 5188 (1976).
 - [31] JP Perdew, JA Chevary, SH Vosko, KA Jackson, MR Pederson, D. J. Singh and C. Fiolhais, Phys. Rev. B **46**, 6671 (1992).
 - [32] M. Weinert and J.W. Davenport, Phys. Rev. B **45**, 13709 (1992).
 - [33] VM Amonenko, V. Ye Ivanov, GF Tikhinskij, VA Finkel, Phys. Met. Metallogr., **14**, 47 (1962).
 - [34] N. W. Ashcroft and N. D. Mermin, Solide state physics. Philadelphis: Saunders College, **15-57** (1976).
 - [35] H Krakauer, M Posternak, AJ Freeman, DD Koelling, Phys. Rev. B **23**, 3859 (1981).